

DTIC FILE COPY

AFWAL-TR-89-4002

AD-A204 335



PREDICTION OF SOLDER JOINT FATIGUE LIFE

H.D. Solomon
V. Brzozowski
D.G. Thompson

Martin Marietta Corporation
Orlando, FLA 32855-5837

April 1988

Interim Report

Approved for Public Release; Distribution Unlimited



Materials Laboratory
Air Force Wright Aeronautical Laboratories
Air Force Systems Command
Wright-Patterson Air Force Base, Ohio 45433-6553

89

1 137001

REPORT DOCUMENTATION PAGE				Form Approved OMB No. 0704-0188	
1a. REPORT SECURITY CLASSIFICATION Unclassified		1b. RESTRICTIVE MARKINGS			
2a. SECURITY CLASSIFICATION AUTHORITY None		3. DISTRIBUTION/AVAILABILITY OF REPORT Approved for Public Release; Distribution Unlimited			
2b. DECLASSIFICATION/DOWNGRADING SCHEDULE None					
4. PERFORMING ORGANIZATION REPORT NUMBER(S) 88CRD101		5. MONITORING ORGANIZATION REPORT NUMBER(S) AFWAL-TR-89-4002			
6a. NAME OF PERFORMING ORGANIZATION Martin Marietta Corp.		6b. OFFICE SYMBOL (if applicable)	7a. NAME OF MONITORING ORGANIZATION Materials Laboratory (AFWAL/MLTE) Air Force Wright Aeronautical Laboratories		
6c. ADDRESS (City, State, and ZIP Code) P.O. Box 5837, Orlando, Florida 32855-5837		7b. ADDRESS (City, State, and ZIP Code) Wright-Patterson AFB, OH 45433-6533			
8a. NAME OF FUNDING/SPONSORING ORGANIZATION Materials Laboratory		8b. OFFICE SYMBOL (if applicable) AFWAL/MLTE	9. PROCUREMENT INSTRUMENT IDENTIFICATION NUMBER F33615-85-C-5065		
8c. ADDRESS (City, State, and ZIP Code) Air Force Wright Aeronautical Laboratories Wright-Patterson AFB, OH 45433-6533		10. SOURCE OF FUNDING NUMBERS			
		PROGRAM ELEMENT NO 78011F	PROJECT NO 3095	TASK NO 04	WORK UNIT ACCESSION NO 02
11. TITLE (Include Security Classification) Prediction of Solder Joint Fatigue Life					
12. PERSONAL AUTHOR(S) Solomon, H.D., Brzozowski V., Thompson D.G.					
13a. TYPE OF REPORT Interim		13b. TIME COVERED FROM _____ TO _____		14. DATE OF REPORT (Year, Month, Day) April 1988	15. PAGE COUNT 36
16. SUPPLEMENTARY NOTATION Prepared as a Prime Team effort by Martin Marietta, Westinghouse, and General Electric, with Martin Marietta as prime contractor.					
17. COSATI CODES			18. SUBJECT TERMS (Continue on reverse if necessary and identify by block number)		
FIELD	GROUP	SUB-GROUP	low-cycle fatigue, joint failure thermal fatigue, fatigue life		
20	11				
19. ABSTRACT (Continue on reverse if necessary and identify by block number) This study details the procedures used to predict the solder joint life from calculations of the joint strains and low-cycle fatigue data. The fatigue life of chip carrier/printed wiring board joints are predicted and compared to measured values. This prediction utilizes a finite element analysis of the strain distributions in a typical joint acted upon by an imposed displacement. These strains are then used to determine the fatigue life through low-cycle fatigue data. The correlation with joint behavior requires a size effect correction to the low-cycle fatigue lives. This correction is required because typical joint dimensions are smaller than the dimensions of the specimen utilized in the fatigue tests and the fatigue life depends upon the joint size.					
20. DISTRIBUTION/AVAILABILITY OF ABSTRACT <input checked="" type="checkbox"/> UNCLASSIFIED/UNLIMITED <input type="checkbox"/> SAME AS RPT. <input type="checkbox"/> DTIC USERS			21. ABSTRACT SECURITY CLASSIFICATION Unclassified		
22a. NAME OF RESPONSIBLE INDIVIDUAL Preston Opt		22b. TELEPHONE (Include Area Code) (513) 255-2461		22c. OFFICE SYMBOL AFWAL/MLTE	

PREDICTION OF SOLDER JOINT FATIGUE LIFE

H.D. Solomon, V. Brzozowski, and D.G. Thompson

1. INTRODUCTION

The phenomenon of the fatigue of surface mount joints has been the subject of considerable study in recent years [1-11]. This present study aims at predicting the isothermal low-cycle fatigue (LCF) of a leadless Chip Carrier/Printed Wiring Board (CC/PWB) joint from isothermal LCF data and a finite element analysis of the strains developed in the joint. This prediction is compared with fatigue lives measured in tests on actual leadless CC/PWB joints. These joints were made using typical manufacturing procedures and actual chip carriers and printed wiring boards.

The procedures utilized in the calculation are discussed in detail as are any approximations utilized and the methods used to correlate the prediction with the experimentally determined fatigue life. Of particular interest is a size effect which must be considered when applying the LCF data to actual joints. This size effect results from the behavior of thin solder layers tested in shear as compared to more typical tests on bulk specimens tested in tension. The most important aspect of this paper is not the specific correlations obtained between measured and calculated fatigue lives. Rather, what is most significant is the description of the approach that was followed, as this approach enables one to apply the general isothermal fatigue life to joints with different geometries. Thus, this approach is described in considerable detail.

This work was done as part of a U.S. Air Force-sponsored manufacturing technology program, with participation by Martin Marietta Orlando Aerospace, Westinghouse (Defense Electronics and R&D Center) and GE (Avionics and Electronics Systems Division and R&D Center). The finite element analysis of solder joint strains was performed by Westinghouse personnel. The fatigue tests on CC/PWB joints, analysis of the LCF data, development of techniques to predict the fatigue life, and correlation of the experimental data with life predictions was done at the GE R&D Center.

1.1 Procedures

No new experimental data is introduced here, so the reader will be directed to the data sources for the specific details utilized in the tests to acquire that data. It is important, however, to get an overview of what is being done, as several different data sources are utilized.

The calculation of the fatigue life is divided into two distinct parts: the calculation of the strains developed in the joints and the prediction of the fatigue life, N_f , from

these strains. The strains were determined from a finite element analysis of solder joints [12]. The fatigue life - strain correlation was made from isothermal tests on simple solder joints [2-5] (but not CC/PWB joints). This predicted fatigue life is compared to that measured on actual CC/PWB joints [13]. The FEA was done on joints which had the same geometry as the tested joints or bracketed the critical feature of the amount of solder in the fillet.

A simple flow chart illustrating the approach taken here is shown in Figure 1. The FEA uses a displacement Δ and calculates the strain distribution γ_T . These strains are in turn used to calculate N_f via a Coffin-Manson LCF curve developed from the tests on simple solder joints. This life is compared to tests run [13] on actual CC/PWB joints which were subjected to the same sort of displacement, Δ , as was used in the FEA.

The analysis is complicated by the fact that the actual strain distribution in a solder joint is highly nonuniform. Without a simple γ_T , it is necessary to use a cumulative damage sort of approach to calculate N_f for various conditions. The use of the LCF curves is further complicated by a size effect which must be corrected for before it can be used for the prediction of actual solder joint lives. The last set of complications comes in utilizing the proper displacements when correlating Δ for the FEA and for the direct measurement of the joint fatigue life. The FEA utilized a zero to Δ displacement, whereas the fatigue tests were run from $-\Delta$ to $+\Delta$. Furthermore, the Δ utilized in the FEA was a total displacement, whereas plastic displacements were utilized in measuring N_f for the solder joints. It is therefore necessary to correct for the elastic strains and this will be discussed.

I. Finite Element Analysis

The FEA model used for analyzing leadless chip carrier solder joint stresses and strains induced by thermal or mechanical excursions was developed by Westinghouse under the Air Force contract F-33615-82-C-5047 supported by the Wright Patterson Materials Laboratory.

A detailed solder joint FEA model allows the user to define, in great detail, the outer dimensions of one solder joint and then generates a finite element mesh of the solder volume. The model assumes that the solder is attached to the HCC and that this interface is a fixed boundary. A copper pad is attached to the bottom surface of the solder and any deflection due to mechanical or thermal loads is applied to the copper pad. The mesh, material properties of the solder and copper, boundary conditions and loading conditions are input to WECAN [17].

WECAN calculates the detailed strain distribution in the solder joint in question under a set of given loading conditions and allows the user to study the levels of strain and their location.

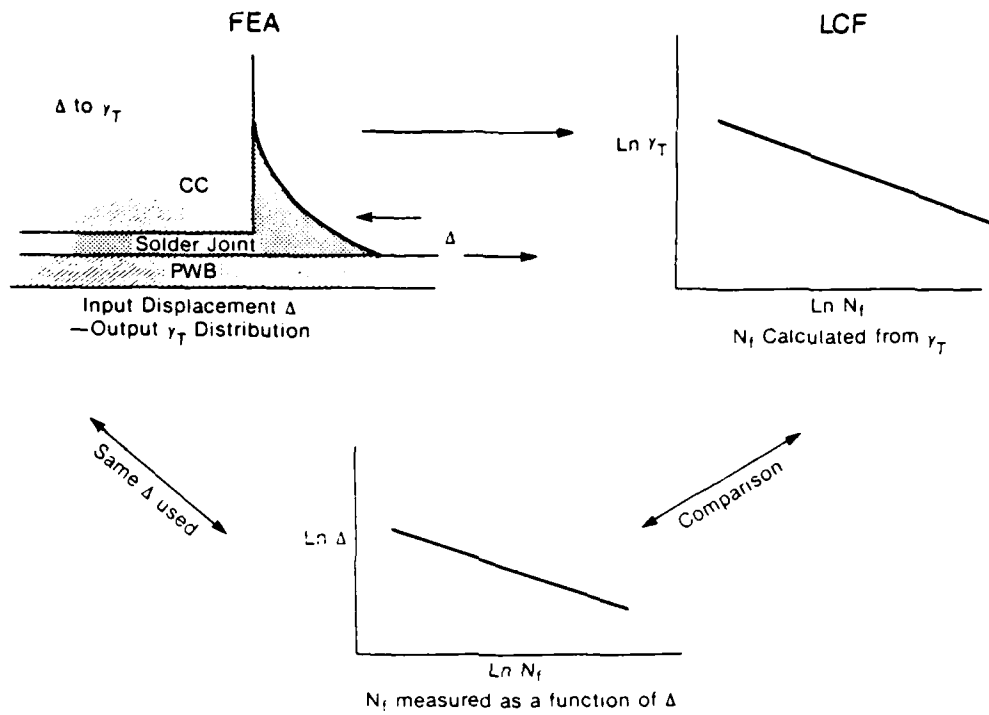


Figure 1. Approach to relate joint strains determined by FEA with strain life LCF data and predict the joint fatigue life.

Visual x-ray and cross-sectional inspection techniques were used to characterize the solder joint geometries fabricated for the LCF tests. Due to manufacturing production variations incurred during sample fabrication, solder joint geometries varied from sample to sample as well as from joint to joint within a sample. The wider variations in solder joint geometry, due to these production variations, make it impossible to analyze every possible configuration. The decision was made that for this set of analysis, the modeling would concentrate on two factors, solder joint height and fillet shape. For the solder joint height (height between the top of the copper pad on the PWB and the metallization on the HCC), heights of 2 mils, 3 mils, and 5 mils were chosen to bracket the cross-sectional heights reported in the microsection work with the 3 mil height acting as a nominal or baseline height. Two solder joint fillet sizes were chosen, a bulbous or full fillet and a minimal fillet, shown in Figures 2 and 3.

The elastic properties required for the copper and solder used in the analysis are contained in Table 1. The plastic properties of the solder (i.e., stress/strain curves) used are given in Figure 4. These curves were developed from bulk 63-37 solder specimen tensile tests performed at Westinghouse under contract number F-33615-82-C-5047. The testing involved a cast ingot of solder which underwent isothermal cyclic testing [16].

The FEA used data obtained from tests on actual Chip Carrier/PWB joints to set the parameters of the model. These were the same specimens used for the isothermal LCF tests [13]. The loading of the specimens was nominally in simple shear and this was the assumed loading for the FEA. The total elastic plus plastic deflection measured by the LCF test extensometers within the first few cycles of the test was used as a basis to calculate the imposed deflections used in the analyses.

It was assumed that the measured deflection was equally divided between each row of solder joints and that the deflection was equal in both the tensile and compressive load cycle, (P^+ and P^-). The imposed deflection in each direction on any one solder joint during the analysis was thus calculated by taking 1/4 of the total deflection from tip to tip of the elastic and plastic hysteresis loop. In addition, each solder joint model analysis had attached to the model, in the direction of the loading, a spring with a very large spring constant (see Figure 5A). The deflection imposed on the solder joint causes the spring to deflect and the deflection of the spring times the spring constant gives the loading on the spring. The high spring constant was chosen such that the deflection in the spring was much less than the deflection in the solder joint. Since the spring is in parallel with the solder joint, this is the loading applied to the solder joint which deflects it a prescribed amount.

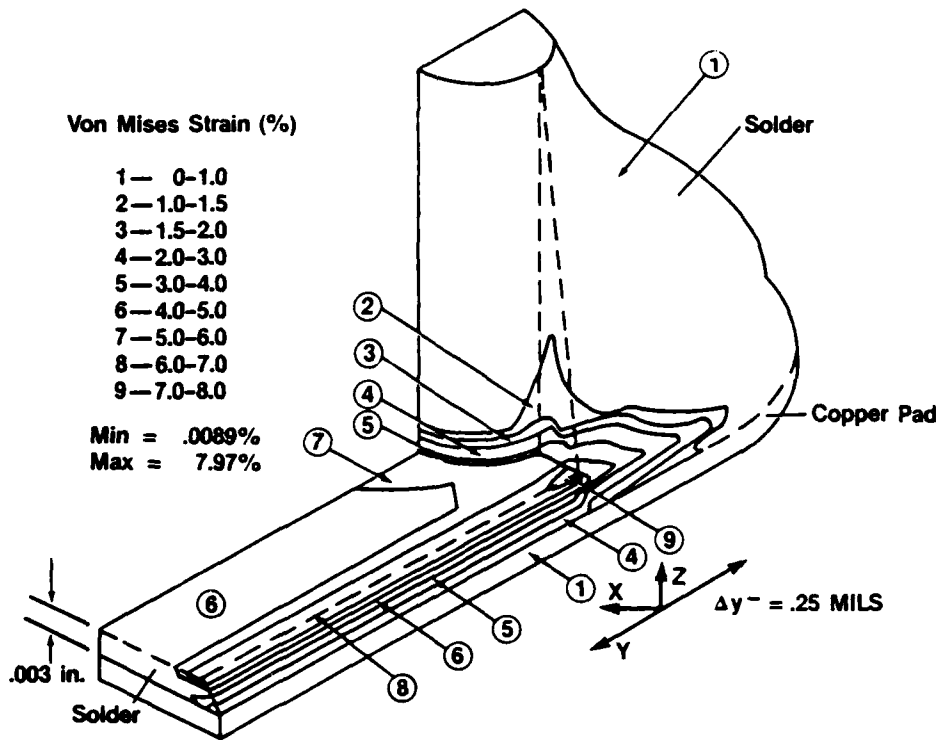


Figure 2. FEA determined strains for a bulbous joint.

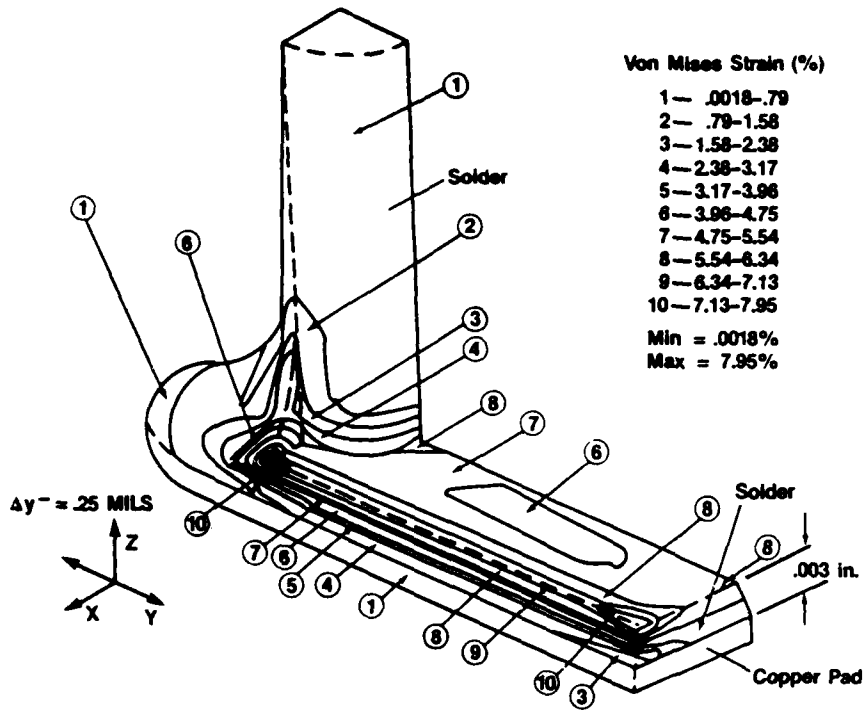


Figure 3. FEA determined strains for a minimal joint.

Table 1
Copper and Solder Elastic Properties Used in Computer Analyses

	Copper	Solder SN63
Coefficient of Thermal Expansion	10.5×10^{-6}	15.7×10^{-7}
Poisson's Ratio	.36	.35
Elastic Modules	17×10^6	3.6×10^6

Note:

Since the HCC to solder joint interface is considered to be a fixed surface, the value of the CTE for the HCC 6×10^{-6} in/in/°C must be subtracted from the values for solder and copper when performing any thermal stress analysis.

STRESS/STRAIN CURVES

TEMP = 105°C

PT	STRAIN	STRESS
1	.5249 E-3	1900
2	.1070 E-2	2150
3	.1620 E-2	2200
4	.3550 E-2	2260
5	.1900 E-1	2450

TEMP = 24°C

PT	STRAIN	STRESS
1	.5003 E-3	1811.
2	.1070 E-2	3875.
3	.1620 E-2	4490.
4	.3550 E-2	4995.
5	.1900 E-1	5000.

TEMP = -55°C

PT	STRAIN	STRESS
1	.4907 E-3	1740.
2	.1070 E-2	3724.
3	.1620 E-2	5638.
4	.3550 E-2	7900.
5	.1900 E-1	9420.

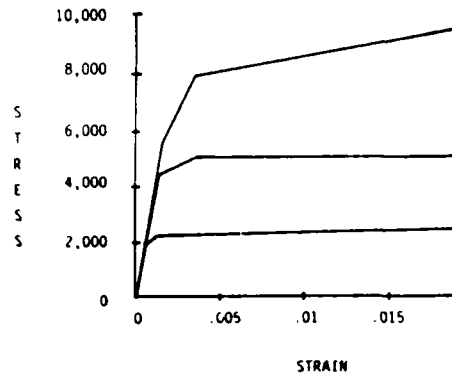
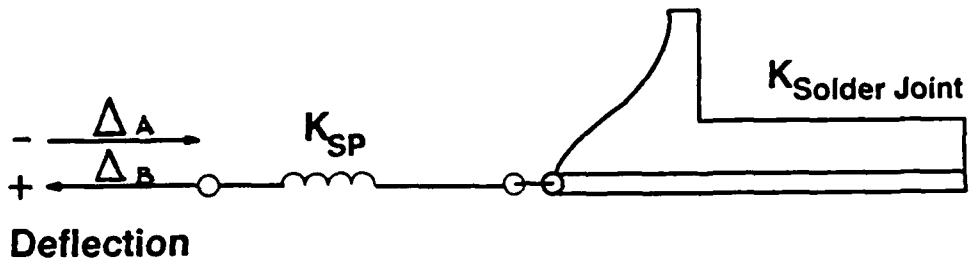


Figure 4. Stress/strain input data.

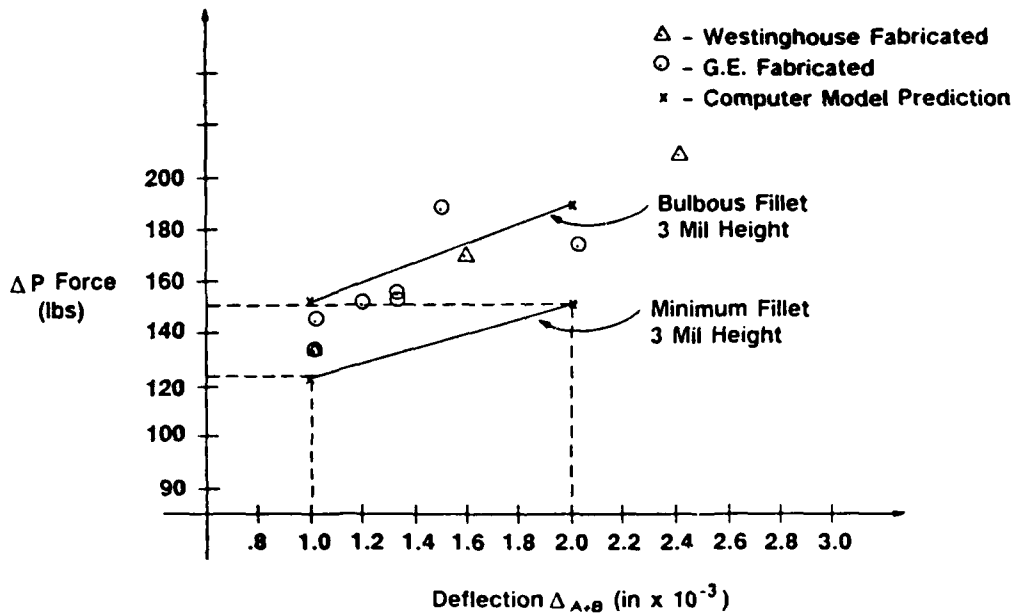
Spring Element Determines Load Solder vs Deflection Solder



$$K_{SP} \gg K_{Solder}$$

Deflection Spring << Deflection Solder
Load Spring ≈ Load Solder

(a)



(b)

Figure 5. a. Spring attachment to solder joint, b. Correlation of LCF test data to modeling prediction.

Figure 5B plots the computer calculated change in force ΔP vs. total deflection $\Delta(A+B)$ across two rows of 11 solder joints which are 3 mils high with a bulbous fillet and 3 mils high with a minimal fillet. Superimposed on these values are data points from samples manufactured by GE and Westinghouse which had undergone the LCF test. The calculated force values bracket the actual test data very well. The data correlation gives confirmation as to the validity of the FEA model and the calculated strain in the FEA solder joint.

Examples of the results of the FEA analysis are given in Figures 2 and 3. These 1/2 models detail the Von Mises strain levels induced in a 3 mil, high minimal and bulbous solder joint undergoing a total deflection of .25 mils in the y direction. An in-depth analysis of the findings of the FEA Analysis are contained in Ref. 12. The following sections of this paper discuss the LCF tests and correlate the measured fatigue lives to the induced strain levels predicted by the FEA analysis.

II. Low-Cycle Fatigue Analysis

The calculation of the total shear strain γ_t enables one to estimate the fatigue life. A complication arises, however, because there is no single γ_t which defines the joint strain. Tests run on actual joints have shown that the initial cracking occurs under the chip carrier, where the strain is the highest. The cracks then propagate into the fillet where the strains are lower. Figure 6 illustrates this schematically. Cracking under the chip carrier occurs due to the application of strain γ_1 . N_1 cycles are required to produce a crack length L_1 . The strain in the transition into the fillet is γ_2 , requiring N_2 cycles to run a crack length L_2 . The final stage in failure consists of growing the crack through the fillet where the strain is γ_3 , length L_3 , requiring N_3 cycles.

Table 2 lists γ_1 , γ_2 and γ_3 for the thin and bulbous fillet joints analyzed in Figures 2 and 3. These strains are the estimated weighted averages over lengths L_1 , L_2 and L_3 . These strains *cannot* be used directly to estimate N_1 , N_2 , or N_3 because they are the VonMises strains, i.e.,

$$\epsilon_{VM} = \frac{\sqrt{2}}{3} \left\{ (\epsilon_1 - \epsilon_2)^2 + (\epsilon_1 - \epsilon_3)^2 + (\epsilon_2 - \epsilon_3)^2 \right\}^{1/2} \quad [1]$$

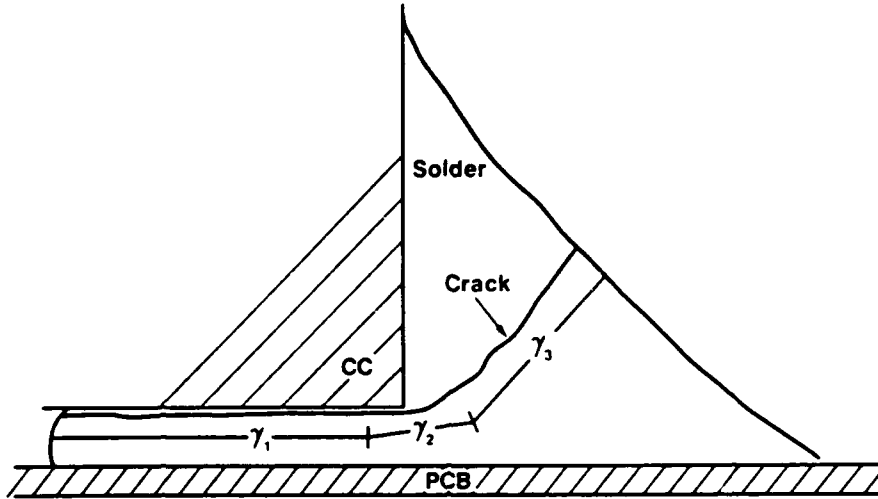
where ϵ_{VM} is the equivalent VonMises strain and ϵ_1 , ϵ_2 and ϵ_3 are the principal strains.

The fatigue life data we will use was generated in shear so we must determine a shear equivalent to the VonMises strain. For pure shear

$$\gamma = \epsilon_1 - \epsilon_2 \quad [2]$$

$$\epsilon_1 = -\epsilon_2, \epsilon_3 = 0 \quad [3]$$

CC/PWB Joint Failure Process



N_1 Cycles under γ_1 strain for L_1 distance
 N_2 Cycles under γ_2 strain for L_2 distance
 N_3 Cycles under γ_3 strain for L_3 distance
 $N_1 \sim 25\%$ load drop
 $N_1 + N_2 \sim 50\%$ load drop
 $N_1 + N_2 + N_3 \sim 100\%$ load drop

Figure 6. Schematic representation of cracking in CC/PWB joints.

Table 2
Strains Developed in Joints

	γ_1 (Under cc)	γ_2 (Transition)	γ_3 (Fillet)
Bulbus (VonMises)	0.050	0.025	0.0050
Minimal (VonMises)	0.055	0.030	0.011
Mean (VonMises)	0.0525	0.0275	0.008
γ_T (Equivalent Shear)	0.091	0.0477	0.0139
$\Delta\gamma_T$	0.182	0.095	0.028

$$\gamma = 2\varepsilon_1 = -2\varepsilon_2 \quad [4]$$

so, from Equations 1-4, we get

$$\varepsilon_{VM} = \frac{1}{\sqrt{3}} \gamma = 0.577\gamma \quad [5]$$

The γ_T (equivalent shear strain) was calculated by dividing the VonMises strains by 0.577 (as per Equation 5). The subscript T is a reminder that the calculation was for the total (elastic + plastic) strain. The mean of the strains in the Bulbus and Nominal geometries is being used because the actual joints were between these two extremes. As can be seen, there is only a modest difference in the strain distribution, so using a mean value is very reasonable.

The last row of Table 2 lists $\Delta\gamma_T$ which is just $2\gamma_T$. The FEA model utilized O to Δ displacements, whereas in testing actual joints a $-\Delta$ to $+\Delta$ displacement range was applied. Symmetry is being assumed because the measured [13] hysteresis loops for tests on actual joints are symmetric, so $\Delta\gamma_T = 2\gamma_T$.

The LCF data utilized the plastic strain range $\Delta\gamma_p$ to correlate the fatigue life [2-5], so it is necessary to correct this data to yield a $\Delta\gamma_T - N_f$ curve, but first we need to consider the $\Delta\gamma_p - N_f$ curves shown in Figure 7. The data on Figure 7 comes from a previous study [2] of single solder joints tested in simple shear (simple shear is, except for a rotation, the same as pure shear, and Equation (5) still holds). In this study a single ≈ 0.0075 in. (0.19 mm) solder layer was used to join Cu or brass blocks. The area soldered was 0.1 in. (2.54 mm) by 0.5 in. (12.7 mm) with the shear in the 0.5 in. direction. No appreciable fillets were made with these joints so the strain could easily be calculated by dividing the applied displacement by the thickness of the solder layer.

Two curve fit correlations are shown in Figure 7. The correlation with $\alpha = 0.52$ (the Coffin-Manson LCF exponent) has been discussed previously [2]. The slope was determined from a least squares fit with a conventional statistical computing package which assumes the ordinate ($\Delta\gamma_p$) to be the dependent variable and curve fits to minimize the deviations from the ordinate coordinates. Unfortunately, the convention with fatigue data is to plot the independent variable $\Delta\gamma_p$ on the ordinate. The solid line (with $\alpha = 0.59$) was calculated by correctly minimizing the deviations from the dependent N_f values. Over the range of the data, there is little difference between the two curves and both give essentially the same life predictions. Extrapolating the data to lower values of $\Delta\gamma_p$ does, however, lead to differences. Differences also arise in correlating with various models used to predict α , but this not a subject to concern us here.

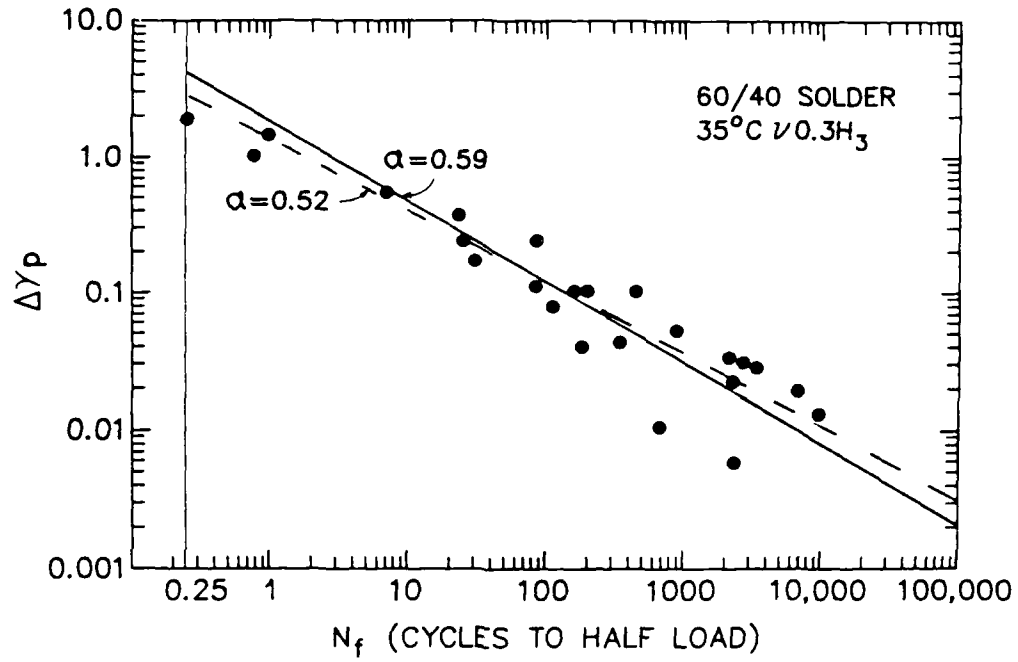


Figure 7. LCF data for 60/40 solder (from Ref. 2). Plastic strain vs. fatigue life (defined by a 50% drop in load).

The $\Delta\gamma_p - N_f$ curve (the correct solid curve of Figure 7) can be converted to the required $\Delta\gamma_T - N_f$ curve by adding the approximate elastic strains, $\Delta\gamma_e$, to the plastic strains, $\Delta\gamma_p$. Care must be taken in making this addition. The elastic strain is dependent upon the stress level which is in turn determined by the deformation rate as well as the amount of deformation. In fact, solders are viscous [4], their flow stress depends upon the strain rate and not just the strain applied. Fortunately strain rate data was generated [4] along with the LCF data. Table 2 lists the shear stress range $\Delta\tau$ required to produce $\Delta\gamma_e = \frac{\Delta\tau}{G}$, where G was calculated from

$$G = \frac{E}{2(1 + \nu)} = 1.2 \times 10^6 \quad [6]$$

with $\nu = 0.5$ (we are in the plastic range) and $E = 4.5 \times 10^6 - 1.5 \times 10^6$ psi depending upon the reference [16,17]. A value of 3.6×10^6 agrees with the value used in the FEA and it yields $G = 1.2 \times 10^6$ psi which is close to the 1.6×10^6 psi value which correlated the data of Reference 2. The data of Table 3 was used to construct the $\Delta\gamma_T - N_f$ curve shown in Figure 8. The $\Delta\gamma_T$ curve was constructed by adding the four $\Delta\gamma_e$ values to the corresponding $\Delta\gamma_p$ values and shifting the $\Delta\gamma_p$ curve (the $\alpha = 0.59$ curve was used because it used the correct curve fitting procedure) to the appropriate $\Delta\gamma_T$ level.

Table 4 lists N_f for the strains $\Delta\gamma_T$, $\Delta\gamma_{T2}$ and $\Delta\gamma_{T3}$ of Table 1 (bottom row). These fatigue lives are *not* the number of cycles to grow a fatigue crack through regions 1, 2 or 3. This is because there is an important size effect that must be taken into consideration.

The fatigue life of Figures 7 and 8 was defined as the number of cycles required to reduce by 1/2 the load required to produce a constant strain per cycle, $\Delta\gamma_p$. The load is reduced because fatigue cycling results in the nucleation and growth of fatigue cracks which reduce the load bearing area. The drop in load represents the amount of cracking. A criteria of, say, a 25% drop in load would correspond to less cracking than that required to produce a 50% drop in load and fewer fatigue cycles would be required for only a 25% drop in load. Likewise, a 90% drop in load (i.e., when the load required to produce $\Delta\gamma_p$ is only 1/10 of that initially required) would necessitate more cycles than that for a 50% drop in load. This presents a problem when utilizing such LCF data. What load drop, or other parameter, should be used to define N_f and what definition allows for the best application of this data? This problem is not a significant one when other materials are tested. This is because most tests are run in tension on materials which are not as ductile as solder, where stable (no change in hysteresis load) hysteresis behavior is noted over a large number of cycles. When the load begins to drop, it generally does so relatively rapidly so that the exact definition used to define N_f does not appreciably influence the data. *This is not the case for*

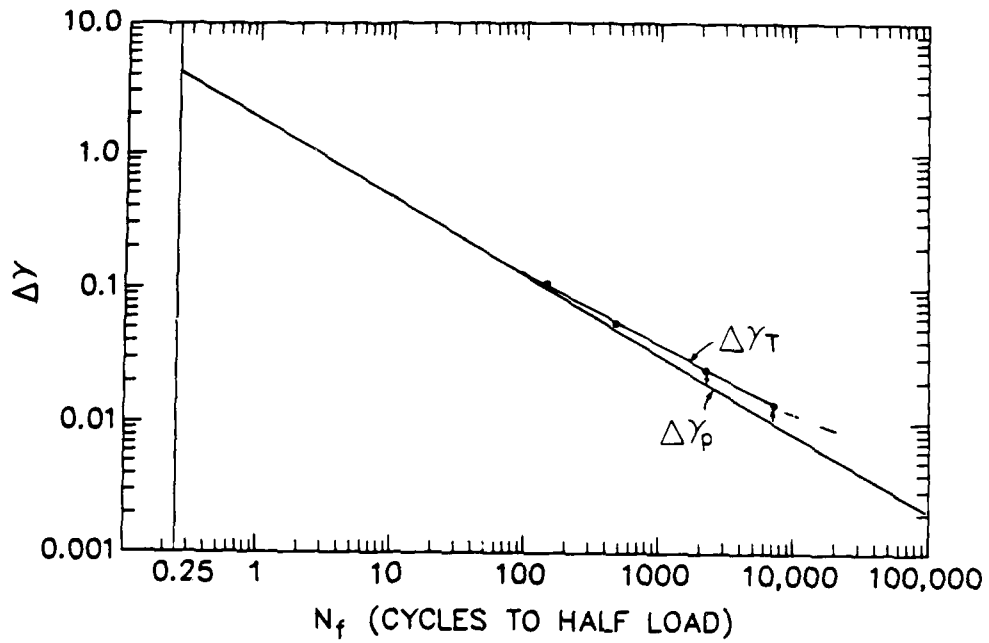


Figure 8. Plastic and total strains vs. fatigue life (defined by a 50% drop in load).

Table 3

Shear Stress, ΔE , for Various Plastic Shear Strains, $\Delta\gamma_p$
measured at 35°C and 0.3 Hz (See Ref. 2).

$\Delta\gamma_p$	$\Delta\tau$ psi	$\Delta\gamma_E$	$\Delta\gamma_T$
0.1	10,000	0.0083	0.1083
0.05	9,000	0.0075	0.075
0.02	7,800	0.0065	0.0265
0.01	6,500	0.0054	0.0154

Table 4

LCF Lives For Strains $\Delta\gamma_{T1}$, $\Delta\gamma_{T2}$ and $\Delta\gamma_{T3}$

$\Delta\gamma_{T1} = 0.182$	$N_f = 54$
$\Delta\gamma_{T2} = 0.095$	$N_f = 180$
$\Delta\gamma_{T3} = 0.028$	$N_f = 1900$

solder tested in shear [2]. In the shear tests performed on solder, the load begins to drop after the first, or at most the first few, cycles and continues to decline, relatively slowly, in a more or less steady manner. The number of cycles required to drop the load by 25% is far less than that required to drop the load by 90%.

It is necessary to correlate the load drop definition of N_f with the amount of cracking required to produce this load drop, so that the cycle life can be normalized to account for the different amounts of cracking. In doing this, the over-riding assumption is that all the load drop is due to cracking and the reduction in area this produces. We are thus assuming that there is no cyclic hardening or softening and that the flow stress remains constant. A drop in load can thus be directly related to a decrease in load bearing area. The assumption that the load drop was due to crack growth was borne out in a qualitative way by ultrasonic microscopy [2]. Figure 9 (taken from Reference 2) shows an example of the results of an ultrasonic microscopy of a sample which was cycled, removed for examination, recycled, re-examined, etc. until final failure. The parameter $\phi = 1 - \frac{\Delta P}{\Delta P_{\max}}$ defines the load drop. It is equal to 0 (i.e., 0 load drop) at the start of the test where $\Delta P = \Delta P_{\max}$ and 1 (100% load drop) when $\Delta P = 0$. The inserts show the microscopy results. The 0.1 in. \times 0.5 in. joint area is outlined (with the shearing in the 0.5 in. direction). The dark areas are the regions which the microscopy delineates as cracked. As can be seen, as the cycling progresses, the cracks grow. Unfortunately, the quality and resolution of the ultrasonic micrographs does not permit a quantitative analysis (all of the cracking is probably not being resolved).

In order to correlate the load drop ϕ with a crack length, it is necessary to make some assumptions and simplifications regarding the geometry of the cracks. If it is assumed that the cracks go across the 0.1 in. joint width and propagate in the 0.5 in. length direction, then the load drop can be correlated with a crack length [2]. A drop in load of 50% ($\phi = 0.5$) requires a crack length of 0.25 in. (one-half the 0.5 in joint length) if a single crack propagates from one end of the joint or 0.125 in. if two cracks are present, one growing from each end. Figure 9 shows that both of these assumptions are simplifications of the actual behavior. The single crack assumption is better at large load drops where the cracks have coalesced and a single crack may dominate, but at very small load drops more than two cracks may be present.

N_f can be corrected for crack growth by considering the average crack growth $\frac{\Delta a}{\Delta N}$. It has been shown [2] that $\frac{\Delta a}{\Delta N}$, as inferred from the drop in load with cycling, is primarily a function of the applied strain $\Delta\gamma_p$. For a constant $\Delta\gamma_p$, $\frac{\Delta a}{\Delta N}$ is thus constant. (This is strictly true only for $\Delta\gamma_p$ at 25% or greater, at lower strains $\frac{\Delta a}{\Delta N}$

decreases with cycling. This effect is corrected for and will be discussed later). For 0 to N_f cycles, i.e., $\Delta N = N_f$, and a crack growth of D , i.e., $\Delta a = D$.

$$\frac{\Delta a}{\Delta N} = \frac{D}{N_f} \quad [7]$$

If $\frac{\Delta a}{\Delta N}$ is just a function of $\Delta\gamma_p$, then for any constant $\Delta\gamma_p$, D/N_f can be related to the number of cycles, N_i , to grow a crack through a distance L_i by

$$\frac{D}{N_f} = \frac{L_i}{N_i} \quad [8]$$

Equation 8 can be rewritten as

$$N_i = \frac{L_i}{D} N_f \quad [9]$$

which enables one to calculate N_i from L_i , D and N_f . Equation 9 correlates N_f as measured from Figure 8 with the amount of cracking, D , used to define N_f and the size of the crack, L_i , which defines N_i .

Now we can estimate the fatigue life for the process depicted in Figure 6. Let us first consider the cracking under the Chip Carrier (i.e., region 1 in Figure 6). Measurements of the CC/PWB geometry show that the length of the solder under the Chip Carrier, L_1 , is 0.04 in. and that the strain in this region $\Delta\gamma_T = 0.182$ in. (see Table 2). If this strain were to have been applied to the simple solder pads, whose fatigue behavior is described in Figures 7 and 8, then the number of cycles, N_f , to reduce the load by 50% is given in Table 4, i.e., $N_f = 54$ cycles. The number of cycles to grow the crack under the Chip Carrier, N_1 , from Equation 9, i.e.,

$$N_1 = \frac{0.04(54)}{D} = \frac{2.16}{D}. \text{ Since } N_f \text{ was defined by a 50\% drop in load for an 0.5 in.}$$

long solder joint, the largest value for D is 0.250 in. This corresponds to a single crack growing through the pad. Figure 9 shows that D should be smaller than 0.250 in,

reflecting the existence of multiple cracks. For four cracks, $D = \frac{0.250 \text{ in}}{4} = 0.0625$

in., which represents a D value which should be at the low end of the probable values for D for cracks which produce a 50% drop in load. Multiple cracking is even more pronounced at the start of the test, but less so at the end of the test where more crack coalescence has taken place. The number of cycles to grow the crack into the fillet, N_2 , and through the fillet N_3 can be calculated in a similar manner. These results, with $D=0.062$ in. and $D=0.250$ in., are summarized in Table 5. The lengths L_2 and L_3 were estimated from the Chip Carrier geometry and the FEA strain distribution (which was used to separate the transition region from the rest of the fillet). The N_f

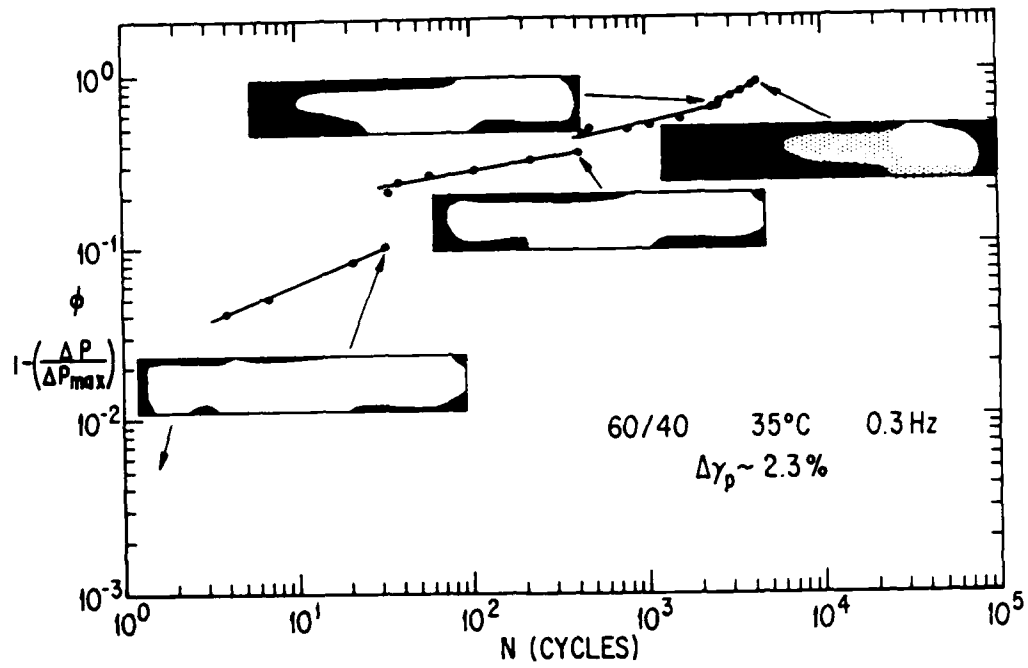


Figure 9. Correlation of ultrasonically measured cracked areas and the drop in load measured in interrupted tests.

Table 5
Calculation of N_i from N_f , L_i and D

	L_i	N_f	D	N_i	D	N_i
$i = 1$	0.04 in	54	0.0625	35	0.250	9
$i = 2$	0.01 in.	180	0.0625	29	0.250	7
$i = 3$	0.015 in.	1900	0.0625	456	0.250	114

values were determined from the $\Delta\gamma_{Ti}$ values as shown in Table 4. N_i not N_f is correlated with the results of fatigue cycling actual joints.

As has already been noted, $\frac{\Delta a}{\Delta N}$ is not only a function of $\Delta\gamma_p$. At strains below 25%, $\frac{\Delta a}{\Delta N}$, as determined from the load drop, decreases with increasing number of cycles. This gives rise to differences in the $\Delta\gamma_p - N_f$ curves when different choices are made for the definition of N_f . Figure 10 shows such curves for N_f defined by a 25%, 50% and 90% drop in load criteria (the data for the 50% curve is shown in Figure 7). As can be seen, α decreases when the load drop definition for N_f increases. This occurs because the lower the strain, $\Delta\gamma_p$, the more the rate of load drop decreases with cycling, producing a decrease in $\frac{\Delta a}{\Delta N}$. (A separate publication is currently being prepared to describe the relationship of α and the degree of load drop used to define N_f). The $\Delta\gamma_T$ curves, created from the calculated $\Delta\gamma_e$ are also shown in Figure 10 and can be used to calculate N_f for a 25%, 50% and 90% drop in load. The results are listed in Table 6 for the same $\Delta\gamma_T$ values used in Table 4. N_1 , N_2 and N_3 can likewise be calculated in the same way as before, i.e., by Equation 9. The results of such calculations are listed in Table 7. There is good agreement between the N_1 , N_2 and N_3 values derived from the 25%, 50% and 90% $N_f - \Delta\gamma_T$ curves of Figure 10, providing the correct value is assigned to D .

A single crack across the joint width would have to grow 0.125 in to produce a 25% drop in load. As noted, however, in the initial stages there are many cracks growing so 0.125/5 or 0.021 in was used to define D . By the time the crack has grown to reduce the load by 50%, there has been a coalescence of the cracks. It is thus assumed that three cracks have grown through the 0.25 half-length, so $D = \frac{0.25}{3} = 0.083$ in. There is further coalescence as the cracks grow, so that by the time a 90% drop in load is reached, there is one dominant crack. It is thus assumed that 1-1/2 cracks are growing through a 0.45 in. length, so $D = \frac{0.45}{1.50} = 0.30$ in. The choice of an increasing D value with load drop and the reduction in slope of the $\Delta\gamma - N_f$ curves with increasing load drop corrects for the error introduced by assuming $\Delta a/\Delta N$ was *only* a function of $\Delta\gamma_p$. If this were the case, the $\Delta\gamma - N_f$ curves should be parallel and spaced according to the load drop used to define N_f (i.e., the 50% load drop curve would be positioned at twice the number of cycles as the 25% curve). The N_i values listed in Table 7 will be compared to the fatigue lives measured in tests of actual CC/PWB joints.

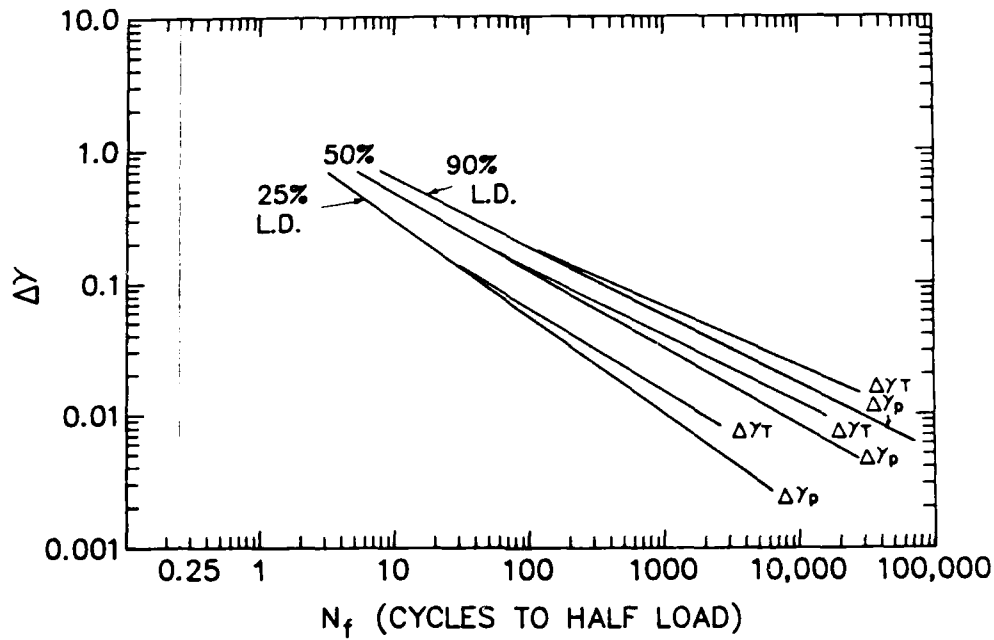


Figure 10. LCF curves ($\Delta\gamma_p$ and $\Delta\gamma_T$ vs. N_f) for N_f defined by a 25%, 50% and 90% drop in hysteresis load.

Table 6
Fatigue Life for N_f defined by Different Drops in Load

$\Delta\gamma_T$	N_f (25%)	N_f (50%)	N_f (90%)
0.182	20	54	110
0.095	52	180	450
0.028	350	1900	6000

Table 7
Calculation of N_i for N_f Defined by Different Drops in Load and Values for D

	$N_1(L_1=0.04 \text{ in.})$	$N_2(L_2=0.01 \text{ in.})$	$N_3(L_3=0.015 \text{ in.})$
For N_f (25%)			
D = 0.021 in.	38	26	250
For N_f (50%)			
D = 0.083	25	22	343
For N_f (90%)			
D = 0.30	15	15	300

III. Comparison with CC/PWB Joint Tests

The main reason why the preceding analysis was performed was to predict the behavior of CC/PWB joint. Such joints have been subjected to LCF by applying shear displacements across the joints. The results of these tests have been discussed extensively [13]. Furthermore, the joints were made with approximately a 3-mil height of the CC above the PWB, which is what was assumed for the FEA calculations. The actual fillet geometry was between the bulbous and nominal geometries, hence the averaging of the calculated strains that was used previously.

There was a difference in the solder and microstructure between that of the LCF data that was used in the calculation and what was used in the actual CC/PWB joints. The previous LCF data utilized 60Sn/40Pb solder with a coarse microstructure. The CC/PWB joint tests utilized 63Sn/37Pb with a finer microstructure. Numerous tests performed in the rest of the Man-Tech program have shown, however, that these are not significant effects insofar as the 35°C isothermal fatigue behavior is concerned (this is what we are trying to correlate). Hence, we shall use the 60/40 LCF data for predictions, without any correction for the slight difference in composition and microstructure between this and that of the CC/PWB joints.

In this section we shall compare the predictions of joint lives made previously with the lives actually measured in the tests on CC/PWB joints. The common thread is that the correlations will be made for the same displacements. Before the test results are considered, it is necessary to correct for the fact that the CC/PWB tests were run with a constant plastic displacement Δ_P , whereas the FEA calculations were done for a given total displacement Δ_T .

The detailed specifics given below refer to the specifics of the experiments that were run and the FEA calculations that were made. They may, therefore, *not* be generally applicable. They have been included, however, not only to illustrate exactly how the life calculations were made, and any approximations that were made, but also to emphasize the importance of making sure that the experimental conditions and FEA assumptions coincide or that any differences are corrected for.

The conversion of Δ_P to Δ_T is complicated by the fact that when Δ_P is kept constant throughout the testing, as was approximately done here, the elastic displacement decreases due to the drop in load which accompanies the cycling. It is therefore necessary to determine the relationship of Δ_P and Δ_T at various stages during the test and correlate this with the number of fatigue cycles reached by that point in the test.

The elastic displacement is determined by the elastic compliance K_o , i.e.,

$$\Delta_E = K_o(\Delta_{load}) \quad [10]$$

This compliance contains displacements of the solder, PWB, CC and any bending that was present. Measurements [13] were made on an uncut PWB with no CC or solder

joint. These measurements and calculations of the elastic behavior of the PWB and CC yielded the result that the compliance due to the solder alone was given by

$$K_S = 0.68K_o \quad [11]$$

so the elastic compliance due to the solder Δ_{ES} is

$$\Delta_{ES} = 0.68K_o(\Delta load) \quad [12]$$

Since all the plastic flow is due to the solder (the tests on the uncut PWB showed that for loads in excess of what was actually used, the PWB behaved elastically) the total displacement used in the FEA can be related to the measured plastic displacement and load range by:

$$\Delta_T = \Delta_P + 0.68K_o(\Delta load) \quad [13]$$

Figure 11 shows the load range $\Delta(\text{load})$ as a function of the plastic strain range, both of which were measured at the start of the test. The data was taken at the start of each experiment and represents the behavior of each test sample. The displacement Δ_P was measured across *both* rows of joints. This is the displacement developed by thermal mismatch and the displacement utilized in most experiments. It is not, however, the displacement utilized in the FEA. There the displacement, Δ_{PS} , across a single row of joints, was considered. At the start of the test, in the symmetrically prepared joints utilized here, the applied displacement was more or less equally distributed between the two rows of joints [13]. By using an arrangement which allowed the measurement of the displacements across each row separately it was found that

$$\Delta_{PS} = 0.49\Delta_P \quad [14]$$

where Δ_{PS} is the plastic strain measured across the single row of joints which eventually fails. The compliance measured across a single row of joints, at the start of a test, is also about one-half that measured across both rows of joints. The elastic displacement of the solder across a single row, Δ_{ESS} is thus (using a 0.49 correction factor)

$$\Delta_{ESS} = 0.33K_o\Delta(\text{load}) \quad [15]$$

The total displacement, Δ_{TS} , measured across a single row of joints is therefore

$$\Delta_{TS} = \Delta_{PS} + \Delta_{ESS} \quad [16]$$

$$\Delta_{TS} = \Delta_{PS} + 0.33K_o\Delta(\text{load}) \quad [17]$$

$$\Delta_{TS} = 0.49\Delta_P + 0.33K_o\Delta(\text{load}) \quad [18]$$

Equation 16 relates Δ_{TS} , which was used in the FEA with the plastic and elastic displacements of the solder of a single row of joints. Equations 17 and 18 relates Δ_{TS} with the compliance measured across both rows of joints, the plastic strain measured across both rows of joints and the load range of the initial hysteresis loop. The plastic

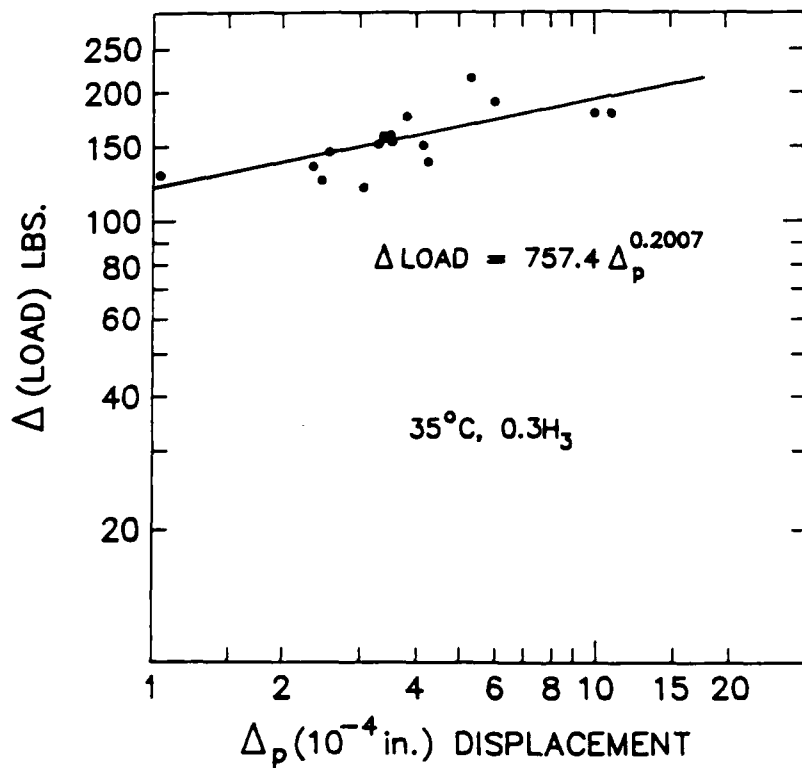


Figure 11. Load range of the initial hysteresis loops vs. applied plastic displacement Δ_p .

strain Δ_P and the load range $\Delta(\text{load})$ are correlated by the data of Figure 11. The best fit to this data yields:

$$\Delta(\text{load}) = 757.4\Delta_P^{0.2007} \quad [19]$$

or for the measured [13] value of $K_o = 7.20 \times 10^{-6}$ in/lb.

$$\Delta_{TS} = 0.49\Delta_P + 1.80 \times 10^{-3}\Delta_P^{0.2007} \quad [20]$$

Equation 20 relates Δ_{TS} (used in the FEA) with Δ_P (used as the control limit for the tests on the CC/PWB joints).

The constants were derived for the start of the test. They change, however, with continued cycling. As the cycling continues, the joints crack. This causes the load required to produce a given Δ_P to decrease and the compliance to increase. Because much of the measured compliance is not due to the solder deflections and generally only row of joints cracks (resulting in a compliance change only for that row), the compliance change is much less than would be expected from the load drop (i.e., when the load drops in half the compliance does *not* double).

The decrease in compliance causes the applied Δ_P to decrease slightly. The tests were run with Δ_P limits with Δ_P being determined by the initial compliance. The change in compliance results in not enough elastic strain being subtracted from the total strain signal and a decrease in the control Δ_P (see Reference 13 for more discussion of this effect). Figure 12 shows the increase in K (as measured across both joints) and the Δ_P decrease resulting from this K increase. Also shown is K_S the compliance measured across the joint that failed. Because the cracking is concentrated in this row, K_S shows a larger increase than K . Also shown is Δ_{PS}/Δ_P which shows how the plastic strain becomes concentrated in the row of joints which crack. All the variables (except Δ_{PS}/Δ_P) are shown relative to the initial values measured at the start of the test. Figure 12 shows how K/K_o , K_S/K_{so} , Δ_P/Δ_{PO} and Δ_{PS}/Δ_P vary with cycling as defined by the drop in load. There is, however, relatively little change in any of these variables below about a 50% drop in load.

The data of Figure 12 can be utilized to correlate Δ_{TS} with Δ_P or Δ_{PS} for any load drop. Equation 20 can be written as a generalized expression

$$\Delta_{TS} = \left[\frac{\Delta_{PS}}{\Delta_P} \right] \Delta_P + \left[\frac{\Delta_{PS}}{\Delta_P} \right] 0.68 \left[\frac{K}{K_o} \right] K_o \Delta(\text{load}) \quad [21]$$

where the expressions in the brackets are described in Figure 12. One further correction is required because $\Delta(\text{load})$ is in general not given entirely by Equation 19. This expression describes the load at the beginning of the test. For any load drop LD , it must be corrected by a $(1 - \frac{LD}{100})$ factor, (i.e., the load is reduced by 0.75 for a 25% load drop). Substituting this factor and Equation 19 into Equation 21, one gets

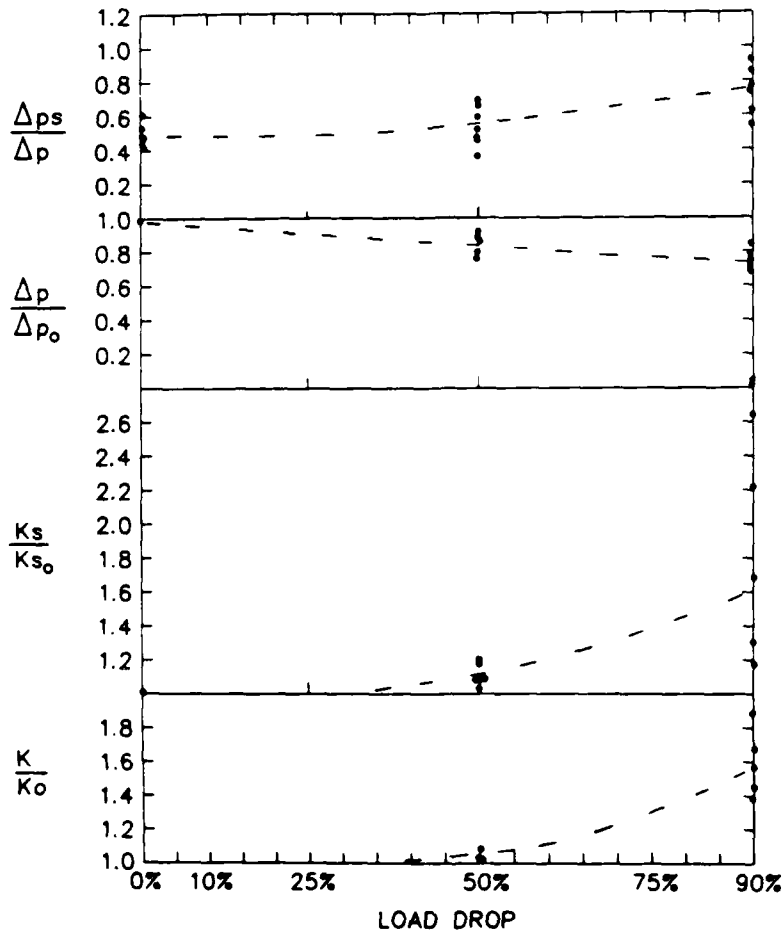


Figure 12. Changes in the compliance, compliance across the joint that is cracking, plastic strain range and plastic strain across the joint that is failing vs. the % drop in load.

$$\Delta_{TS} = \left(\frac{\Delta_{PS}}{\Delta_P} \right) \Delta_P + \left(\frac{\Delta_{PS}}{\Delta_P} \right) 0.68 \left(\frac{K}{K_o} \right) K_o \left(1 - \frac{LD}{100} \right) 757.4 \Delta_P^{0.2007} \quad [22]$$

Equation 22 is a generalized expression which relates Δ_{TS} with Δ_P for any load drop (Equation 20 is valid only for the start of the test where $\Delta_{PS}/\Delta_P = 0.49$, $\frac{K}{K_o} = 1$, and $LD = 0$). This equation enables us to relate the FEA performed for a given Δ_{TS} with the CC/PWB tests performed with Δ_P limits for any point in the test (i.e., for any drop in load). The fatigue life was measured for 25%, 50% and 90% drop in load.

Figures 13 and 14 show the results for N_f defined by a 25% drop in load. For this drop in load, $K/K_o = K_S/K_{SO} = 1$, $\Delta_P/\Delta_{PO} \approx 1$, and $\Delta_{PS}/\Delta_P \approx 0.49$. Only the load drop term is appreciably different from its initial value. It decreases to 0.75 from 1, so an average value of 0.875 will be used in Equation 22, i.e., with $K_o = 7.20 \times 10^{-6}$ in/lb, Equation 22 becomes

$$\Delta_{TS} = 0.49\Delta_P + 1.59 \times 10^{-3} \Delta_P^{0.2007} \quad [23]$$

For $\Delta_{TS} = 5 \times 10^{-4}$ in. (twice the value used in the FEA which considered only 0 to + Δ whereas the experiments were performed for - Δ to + Δ). $\Delta_P = 3.60 \times 10^{-4}$ in. and $\Delta_{PS} = 1.76 \times 10^{-4}$ in. *These are the plastic displacements which correspond to an applied total displacement across one row of joints of 5×10^{-4} in.*

Figures 13 and 14 can be used to determine N_f for these plastic displacements. For N_f defined by a 25% drop in load, these curves yield $N_f = 26$ for the Δ_P data (i.e., with the plastic displacement measured across both rows of joints) and $N_f = 33$ cycles for the correlation with the displacements measured across the row of joints which actually failed. The differences between these two measurements reflects differences in the curve fits to the data. The average value of $\Delta_{PS}/\Delta_P = 0.49$ but the data curves are displaced by a factor of 0.53. The Δ_{PS} correlation is most appropriate for comparisons with the FEA which was done on a single joint. The correlation with Δ_P is given because this is what would be calculated in a thermal displacement calculation. Initially the displacement is equally shared by both rows of joints so $\Delta_P \approx 2\Delta_{PS}$. As the test progresses, however, more of the displacement becomes shared by the row of joints in which cracks are developing.

An examination [13] of specimens has shown that a load drop of 25% correlates with cracking under the chip carrier, i.e., with region 1 of Figure 6. These N_f values should therefore correlate with N_1 from Table 7 (Column 1). The measured value of 26-33 cycles is in excellent agreement with the predicted values of 15-38 cycles (see Table 7).

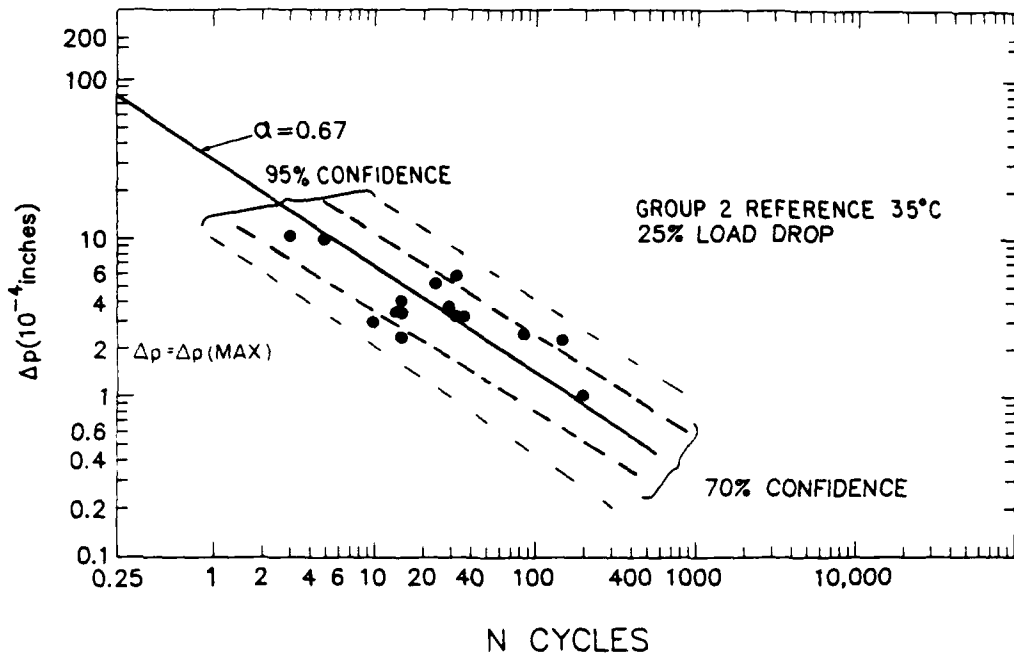


Figure 13. Plastic displacement, Δp , across both rows of joints vs. N_f for a 25% drop in load.

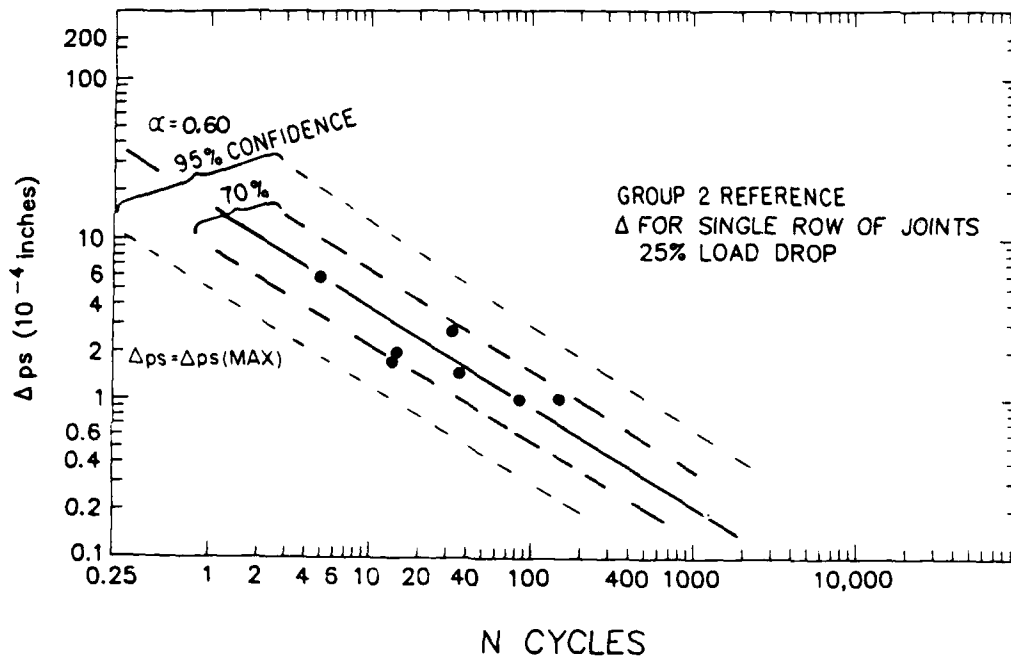


Figure 14. Plastic displacement, Δp_s , across the row of joints that failed vs. N_f for a 25% drop in load.

A drop in load of 50% resulted in cracks which grew into the CC/PWB joint fillet but did not propagate through the fillet. We will therefore correlate this behavior with the number of cycles to grow through regions 1 and 2, i.e., N_f for a 50% drop in load should correlate with $N_1 + N_2$ as listed in Table 7. When the load drops by 50%, there are significant changes in K/K_o , K_s/K_{so} , Δ_P/Δ_{PO} and Δ_{PS}/Δ_P as listed in Figure 12. The average changes from 0 to a 50% drop in load are $K/K_o = 1.02$, $K_s/K_{so} = 1.06$, $\Delta_P/\Delta_{PO} = 0.924$, and $\Delta_{PS}/\Delta_P = 0.525$, $\left[1 - \frac{LD}{100}\right] = 0.75$ (the average LD is 25%). Equation 22 thus reduces to

$$\Delta_{TS} = 0.525\Delta_P + 1.489 \times 10^{-3}\Delta_P^{0.2007} \quad [24]$$

For $\Delta_{TS} = 5 \times 10^{-4}$, $\Delta_P = 3.71 \times 10^{-4}$ and with $\Delta_{PS} = 0.525\Delta_P = 1.95 \times 10^{-4}$. Figures 15 and 16 plot N_f for a 50% drop in load in the CC/PWB joint tests vs. Δ_P and Δ_{PS} . Here the plastic displacements are the averages for zero drop in load to 50% drop in load. For $\Delta_P = 3.71 \times 10^{-4}$ in., $N_f = 64$ cycles and for $\Delta_{PS} = 1.95 \times 10^{-4}$ in., $N_f = 59$ cycles. These results are also in excellent agreement with $N_1 + N_2$ from Table 7, i.e., with 30-64 cycles.

By the time the load has dropped by 90%, cracks are visible in most of the fillets in the CC/PWB joints [14]. This load drop should thus correlate with $N_1 + N_2 + N_3$ of Table 7. The rate in the drop in load slows down after a 50% drop in load is reached [14]. It takes many more cycles to reduce the load from 50% to 90% than to reduce it from 0 to 50%. Thus, instead of considering the average value of the parameters of Figure 12 over 0 to a 90% drop in load, we will use the average from 50% to 90% drop in load and likewise Figures 17 and 18 show N_f defined by a 90% drop in load as correlated by $\frac{\Delta_P(.5) + \Delta_P(.9)}{2}$ and $\frac{\Delta_{PS}(.5) + \Delta_{PS}(.9)}{2}$. For $K/K_o = 1.305$, $K_s/K_{so} = 1.369$, $\Delta_P/\Delta_{PO} = 0.806$, $\Delta_{PS}/\Delta_P = 0.655$ and $\left[1 - \frac{LD}{100}\right] = 0.3$, Equation 22 becomes

$$\Delta_{TS} = 0.655\Delta_P + 9.509 \times 10^{-4}\Delta_P^{0.2007} \quad [25]$$

For $\Delta_{TS} = 5 \times 10^{-4}$, $\Delta_P = 4.54 \times 10^{-4}$ and for $\Delta_{PS} = 0.655$, $\Delta_P = 2.97 \times 10^{-4}$. Because of the drop in load and concentration of the displacement in the row of joints that is failing, Δ_{PS} is approaching Δ_P and Δ_P is approaching Δ_{TS} . For $\Delta_P = 4.54 \times 10^{-4}$ in., $N_f = 285$ cycles and $\Delta_{PS} = 2.97 \times 10^{-4}$ in., $N_f = 280$ cycles. Because of hysteresis loop distortions which developed at large load drops, N_f was also correlated with Δ_P as measured at zero load instead of at the load reversal (see Reference 13). The N_f (90% drop in load) as correlated by this zero load, Δ_P measurement is shown in Figure 19. For $\Delta_P = 4.54 \times 10^{-4}$ in., $N_f = 200$ cycles. These N_f values are in good agreement with $N_1 + N_2 + N_3$ as listed in Table 7 (i.e., 313 to 390 cycles).

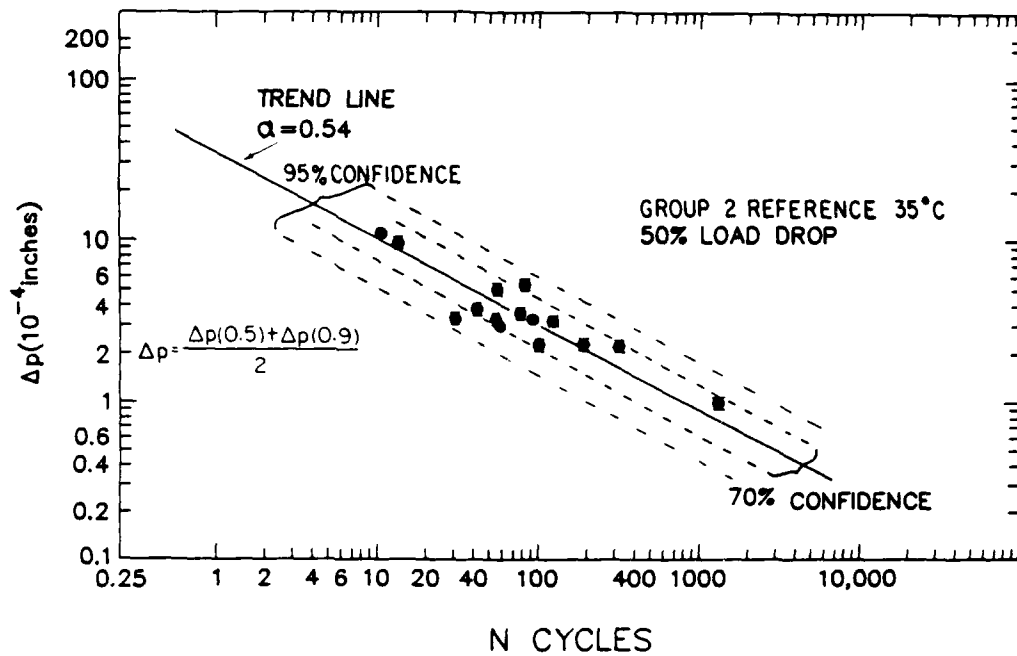


Figure 15. Plastic displacement, Δ , across both rows of joints vs. N_f for a 50% drop in load.

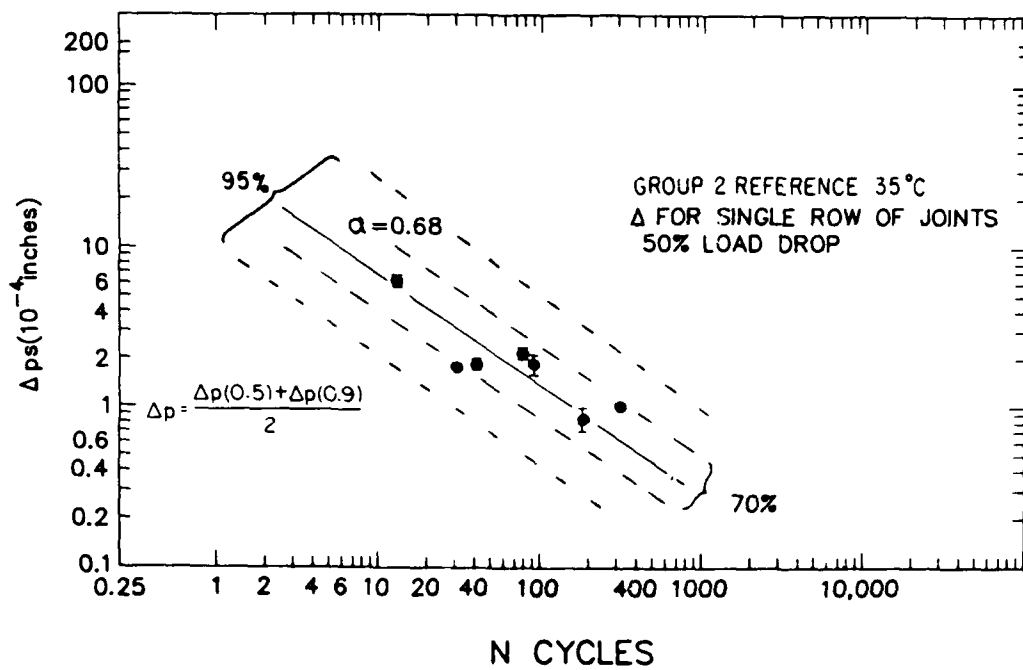


Figure 16. Plastic displacement, Δ_{ps} , across the row of joints that failed vs. N_f for a 50% drop in load.

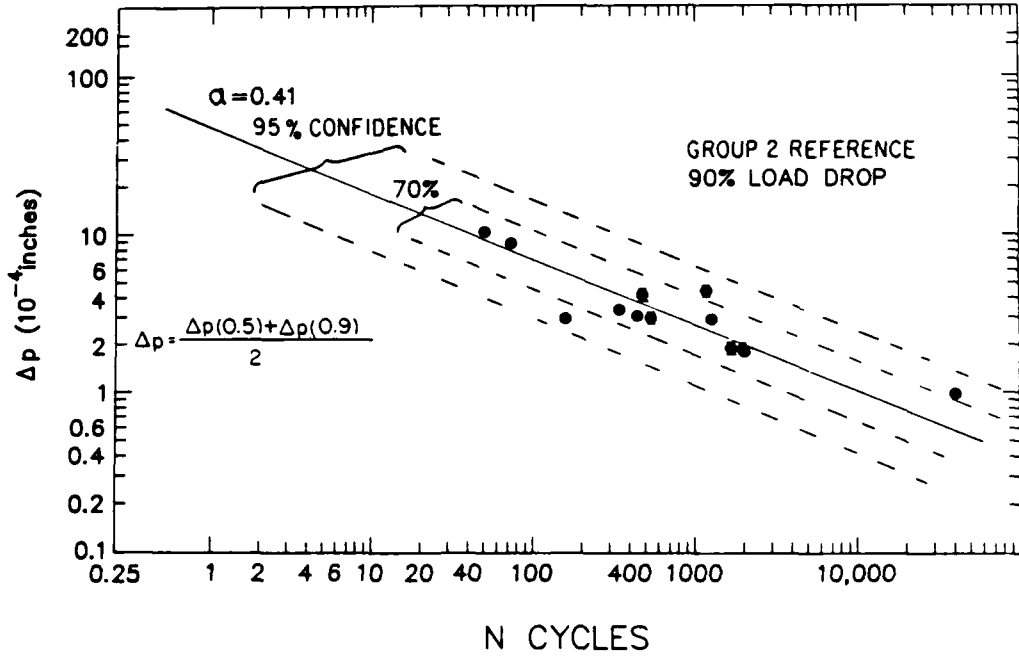


Figure 17. Plastic displacement, Δ , across both rows of joints vs. N_f for a 90% drop in load.

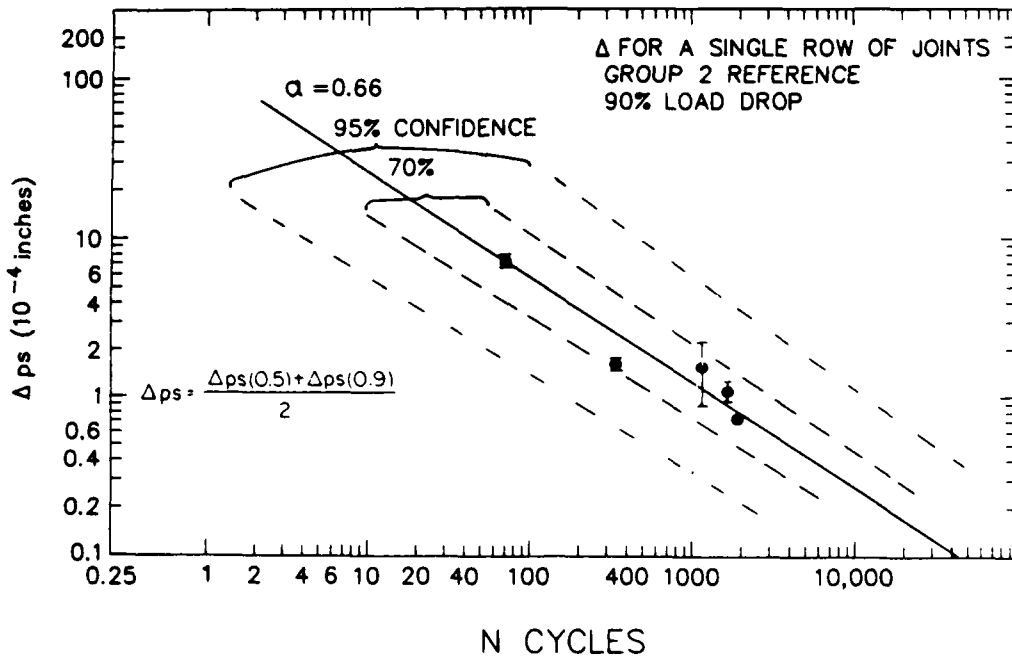


Figure 18. Plastic displacement, Δps across the row of joints that failed vs. N_f for a 90% drop in load.

Figure 20 compares all the predictions and measurements, and illustrates the excellent agreement that has been obtained with predictions falling *within* $\pm 2X$ of the measured values. The measured data was obtained from the Δ_P and Δ_{PS} correlations and the small differences represent curve fit differences to the data. It is important to remember that Δ_{PS} is not just $\frac{\Delta_P}{2}$ and if $\frac{\Delta_P}{2}$ were used to define the behavior of a single row of joints (the condition for which the calculations were made), a serious error would be made. If only Δ_P data were available, some sort of estimate would have to be made to determine how the strains were partitioned. Equal partitioning may be o.k. at the start of the test, but it is not a correct procedure to follow at later lives. The most conservative approach would be to assume $\Delta_P = \Delta_{PS}$ which would yield an underestimate of the actual fatigue life.

The values of D used in Table 7 greatly influence the predicted fatigue lives. The D values were chosen to give the best balance of predicted lives vs. the measured ones. This parameter is *not*, however, just an error minimization factor. It must conform to the size of the pad used in generating the N_f data and to the degree of multiple cracking at any stage in life. The accuracy of the predictions also depends upon the accuracy with which the FEA determines the strain distribution and the degree to which the joint geometry can be specified accurately. Even if a very accurate prediction can be made, at best it will only reflect the mean expected behavior. The scatter in the experimental data is such that the behavior of individual specimens can significantly deviate from this mean.

The scatter in the measured values of N_f can be greater than $3X$, depending upon the confidence limits that are considered. Figures 13-18 show the least squares best fit trend line and dotted lines which define 70% and 95% confidence limits. These are close to but not exactly the same as one and two standard deviation limits. A 70% confidence boundary means that there is 70% confidence that the results for the next test will fall within this band and a 15% probability that it would fall above the boundary and a 15% probability that it would fall below the boundary. Likewise, for the 95% confidence zone, there is a 2.5% probability that the next data point would be below this band. In the data sets with the most scatter, there is a factor of 5 spread between this 95% confidence boundary and the mean. Thus there is a 2.5% probability that a measured value could be only 1/5 the mean value. This is not a particularly surprising fact, nor is the level of scatter particularly large considering the real joints are being tested, not carefully machined specimens. A design which calls for greater than 97.5% confidence requires more than a factor of safety of $5X$ on *measured* mean values.

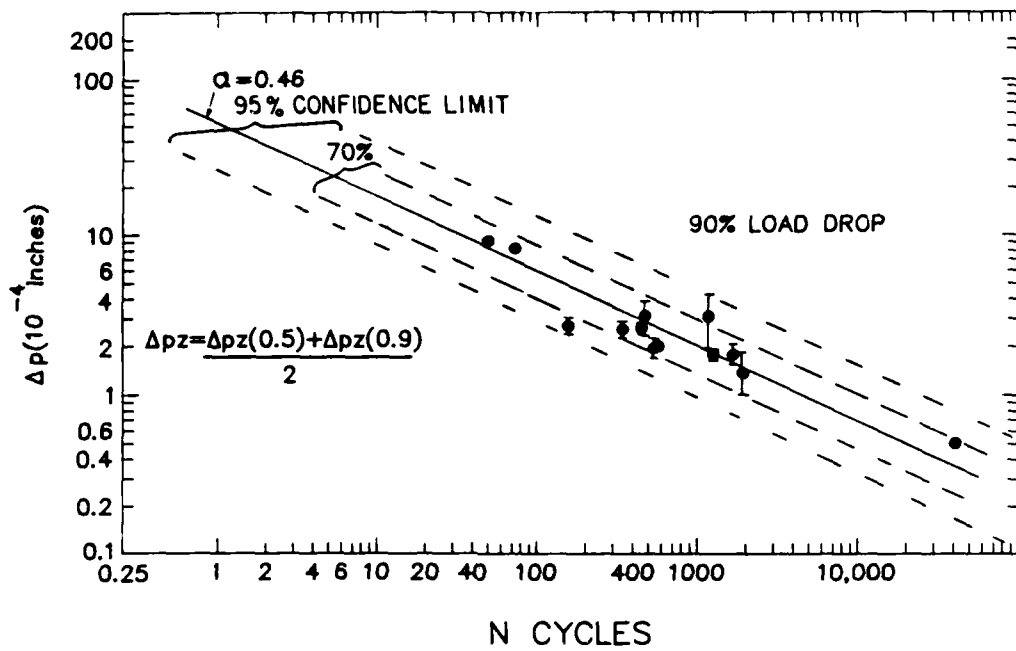


Figure 19. Plastic displacement, Δp_z , across both rows of joints as measured at zero load vs. N_f for a 90% drop in load.

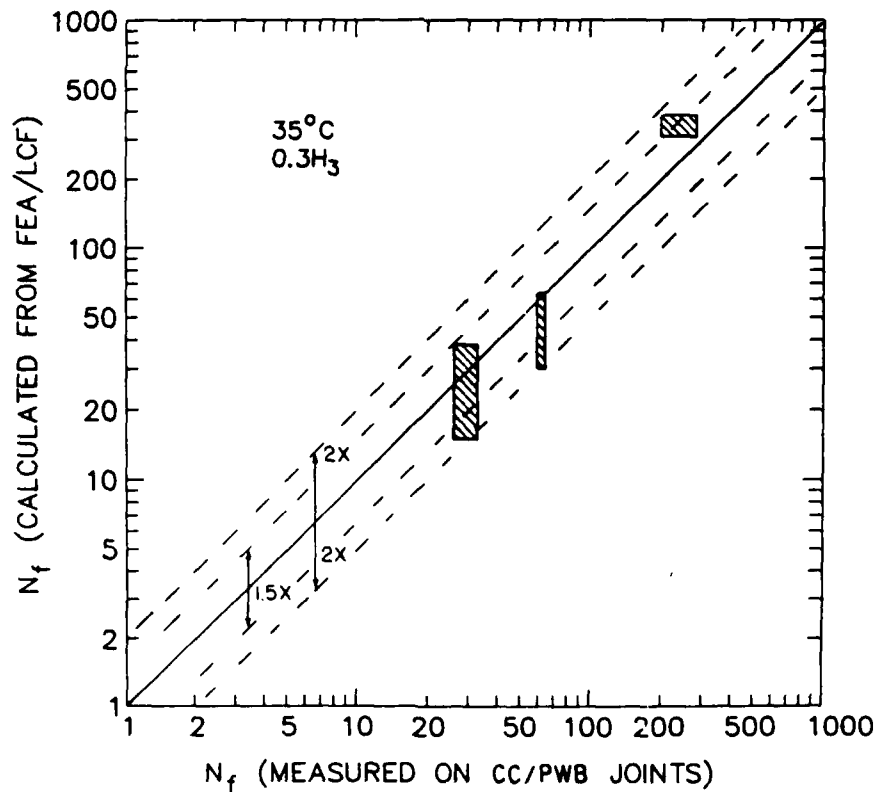


Figure 20. Comparison between the predictions made from the FEA and LCF data and measurements on CC/PWB joints.

The scatter in the data makes it difficult to detect subtle effects such as slight changes in solder composition. Gross changes such as large changes in the fillet geometry can, however, be measured. These effects will be discussed in subsequent Man-Tech papers.

IV. Predicting Thermal Fatigue Lives

All the aforementioned data and discussion refer to tests run at one temperature where the fatigue results from mechanical displacements. While a knowledge of this behavior is critical to predicting the thermal fatigue behavior of CC/PWB joints, it is not enough to make accurate predictions. In this section we shall discuss the methodology for making predictions of the thermal fatigue of joints and some simple approximations that, together with the isothermal approaches described in this paper, could be used to make a first, rough, estimate of the fatigue life. The steps required to make a thermal fatigue life estimate are as follows:

A. Determine the Thermal Displacement

The previous analysis has shown that in order to estimate the fatigue life it is necessary to know the displacement being applied to a solder joint. This is as true for thermal fatigue as it is for the isothermal fatigue considered here. This thermal displacement arises because of the mismatch in the coefficients of thermal expansion, $\Delta\alpha$, between the CC and PWB. In a leadless device, this mismatch is taken up by the solder joint and deflections in the PWB. There is no lead to deflect and take up this displacement. To a first approximation for a temperature change ΔT the thermal displacement can be calculated as

$$\Delta = \frac{(\Delta\alpha)(\Delta T)L_o}{P} \quad [26]$$

where L_o is a CC length dimension, typically the longest distance between solder joints (close to the diagonal length), and P is partition coefficient equal to 2 if the displacement is equal on opposite sides of the chip carrier and equal to 1 if all the displacement is assumed to be on one side. The largest plastic displacement Δ_p is achieved if all the displacement is plastic solder joint displacement and using $P = 1$

$$\Delta_p = (\Delta\alpha)(\Delta T)L_o \quad [27]$$

Equation 27 assumes that all the displacement is taken up on one row of joints and that all of these displacements are plastic. Above room temperature, solder creep relieves any thermal stresses and the assumption that all the displacement is plastic is a good one. Below room temperature, however, there is much less creep and, depending upon the exact temperature and times involved

in the thermal cycling, there may be significant elastic solder strains and deflections of the PWB. As an approximation, it can be assumed that all the fraction of ΔT spent above room temperature, T_R , produces plastic strains but that only $1/B$ of the thermal displacement developed below T_R produces plastic displacements, i.e.,

$$\Delta_P = \left(\frac{T_M - T_R}{\Delta T} + \frac{T_R - T_N}{B \Delta T} \right) \frac{\Delta \alpha \Delta T L_o}{P} \quad [28]$$

(where T_M is the maximum temperature and T_N is the minimum temperature). For equal excursions above and below T_R , i.e., $T_M - T_R = T_R - T_N = \frac{\Delta T}{2}$

$$\Delta_P = \left(\frac{1}{2} + \frac{1}{2B} \right) \frac{\Delta \alpha \Delta T L_o}{P} \quad [29]$$

Furthermore, if $B = 2$ (i.e., half the displacement developed below T_R produces plastic displacement) and $P = 1.5$, which assumes some unequal displacement partition (between $P = 1$ which denoted partition to one side only and $P = 2$ which is equal partition) Equation 29 becomes

$$\Delta_P = 0.5(\Delta \alpha)(\Delta T)L_o \quad [30]$$

which is a reasonable estimate for Δ_P (for equal thermal cycles above and below T_R), but one which may still overestimate Δ_P . The most conservative (largest) simple estimate for Δ_P is given by $P = 1$ and $B = 1$ and is given by Equation 27 no matter how ΔT is distributed above or below T_R .

As a first estimate of Δ_P one should use Equation 26 or 28. If the predicted life plus a safety factor exceeds the design guidelines, then no further calculation of Δ_P is needed. If this is not the case, then a more refined calculation is needed. Equation 29 may overestimate Δ_P because P may be closer to 2 and B closer to ∞ . For $P = 2$ and $B = \infty$, Equation 29 becomes

$$\Delta_P = 0.25(\Delta \alpha)(\Delta T)L_o \quad [31]$$

which is a simple lower bound estimate for Δ_P but not the lowest possible value for Δ_P because it neglects the possibility that some of the thermal strains are taken up by bending the PWB.

Determining the exact value for Δ_P , as opposed to the simple approximations discussed here is difficult, but can be done [8,9,12]. A proper estimate of Δ_P is critical because N_f varies approximately with the square of Δ_P . Thus, there would be a factor of 16 difference in N_f as estimated from Equation 27 vs. Equation 31. A refined calculation of a whole circuit board populated by a large

number of leadless chip carriers and other components might show that even Equation 27 was not an upper bound to Δ_P because PWB bending might be concentrated in a region giving an extra contribution to Δ_P not accounted for in Equation 27. There may also have to be special consideration given to the corner joints as these may also experience additional displacement due to asymmetries in bending, heat transfer, and the largest L_o for the Chip Carrier (i.e., the diagonal length rather than the opposite side length).

The PWB bending causes the chip carrier to experience tensile as well as shear strains, and the chip tends to move up away from the PWB. This complicated displacement pattern should serve as the boundary condition for the calculations discussed below.

B. *Calculation of Strains From the Thermal Displacements*

Once the thermal displacement is determined, the joint strain distribution can be determined by FEA. This calculation is, however, considerably more difficult than the one discussed here. All the elastic and plastic properties vary with temperature. Furthermore, the yielding of the joint will be a function of not only the temperature but also the rate of temperature change, which establishes a strain rate.

This calculation should be due to yield $\Delta\gamma_P$ rather than $\Delta\gamma_T$. In the calculations performed here, it was a relatively simple manner to convert $\Delta\gamma_P - N_f$ curves to $\Delta\gamma_T - N_f$ curves. When the temperature varies, so does the elastic strain (due to differences in the yield strength and elastic modulus). Thus the conversion of $\Delta\gamma_P$ data to $\Delta\gamma_T$ data is difficult and should therefore be done as part of the FEA, where a temperature variation can be incorporated.

The most accurate calculation should employ the complicated displacements, developed because of PWB bending, as the boundary conditions for the calculation. Furthermore, these calculations should also take any metallurgical instabilities into account. In thermal fatigue tests, unlike the isothermal tests discussed here, a grain coarsened or recrystallized zone often develops under the Chip Carrier and extends into the fillet. The mechanical properties of this zone are different from those of the rest of the joint. Strains become concentrated in this zone and are higher than would be estimated were no local metallurgically distinct zone formed. These increased strains will reduce the fatigue life. Thus the formation of a grain coarsened or recrystallized zone is an important factor in determining the fatigue life, and is a factor which an accurate life prediction must account for.

If the mechanical properties of the coarsened or recrystallized zone can be determined, then the FEA can be modified to account for this zone. The FEA

can then yield the strain in this one and these strains can be used, following procedure C below, to calculate N_f .

C. *Calculation of N_f from $\Delta\gamma_P$*

Once $\Delta\gamma_P$ is calculated for the thermal cycle, it is a relatively simple matter to calculate N_f , following the procedures laid out in this report. A distribution of $\Delta\gamma_P$ strains should be considered and N_i calculated for each relevant strain in the distribution. Fortunately there does not appear to be a large influence of temperature on the $\Delta\gamma_P - N_f$ behavior [5], and to a first approximation, room temperature data can describe the behavior over a range of temperatures. *There is, however, a correction which must be made to account for the cycling frequency.* In a typical thermal cycle test this is determined by the rate of temperature change and hold time at temperature. This correction can be quite large, an order of magnitude reduction in the fatigue life at low frequencies, compared to high frequency results, has been observed. A correction should also be made for the asymmetries which develop in thermal cycling, where a much higher stress is reached at low temperatures than at high temperatures [5].

D. *Fatigue Life Criteria*

Assuming one has calculated Δ_P and from it $\Delta\gamma_i$ and from it N_i , one is now ready to define the fatigue life. The question now arises, however, as to what constitutes failure. Failure could be defined as the number of cycles N_1 to grow a crack under the chip carrier, the number of cycles ($N_1 + N_2$) to grow it into the fillet or the number of cycles ($N_1 + N_2 + N_3$) to grow it completely through the fillet. Using N_1 as a design life is very conservative, probably too conservative since if the fillet is uncracked there will be little change in the joint electrical properties [14]. Using $N_1 + N_2 + N_3$ as a criteria is non conservative. This will predict the average behavior but it has been shown [13] that long before the average joint cracks all the way through the fillet the worst joint will have already failed and this, not the average joint behavior, marks the failure of the device.

The best criteria for failure is a resistance increase of 0.1% in the first joint to show such an increase. Above this resistance increase, cracks are clearly observed through the joint fillet. This behavior correlates with a little more than a 50% drop in load, measured in the joint fatigue tests. This in turn correlates with $N_1 + N_2$, i.e., the number of cycles for an average joint to have a crack growing through the transition region into the fillet. This is somewhat conservative because it generally takes a little over a 66% drop in load before the worst joint reaches a 0.1% resistance increase and a visible crack through the fillet [13].

In summary, the suggested design approach is to

- A. Calculate the thermal displacement, Δ_p , using an exact solution if necessary.
- B. Calculate the joint strain distribution $\Delta\gamma_i$ from Δ_p using FEA.
- C. Calculate N_i from $\Delta\gamma_i$ using the LCF data, correcting for frequency and asymmetry effects.
- D. Calculate N_f from N_i , correcting for the joint size effect described here. Define N_f as ΣN_i , $N_f = N_1 + N_2$ is suggested, where $N_1 + N_2$ are the number of cycles to grow a crack into, but not through the fillet of the average joint.

ACKNOWLEDGMENTS

This work was performed under AF Contract No. F33615-85-C-5065. The authors are grateful for this support and for the support given by Don Knapke, Preston Opt and Ed Morrissey, all of the AF Materials Lab (WPAFB, Ohio).

REFERENCES

- [1] J. H. Lau and D. W. Rice, Solid State Technology, V.28, pp.91-104, (1985).
- [2] H. D. Solomon, "Low-Cycle Fatigue of 60/40 Solder-Plastic Strain Limited vs. Displacement Limited Testing" on Electronic Packaging: Materials and Processes, Ed. J. A. Sortell, ASM, pp.29-49, 1986.
- [3] H. D. Solomon, "Low-Frequency, High-Temperature, Low-Cycle Fatigue of 60Sn/40Pb Solder," in A.S.T.M. - STP 942, Ed. H. D. Solomon, et.al., pp. 342-369, 1987.
- [4] H. D. Solomon, Brazing and Soldering, No. 11, pp.68-75 (1986).
- [5] H. D. Solomon, IEEE-CHMT-9, pp. 423-433 (1986).
- [6] W. Engelmaier, IEEE-CHMT-6, p. 232-237 (1983).
- [7] J. K. Lake and R. N. Wild, 28th National SAMPE Symposium, pp.1406-1414, (1983).
- [8] P. M. Hall, IEEE-CHMT-7, pp.314-327 (1984).
- [9] D. Stone, S.P. Hanula and C.Y. Li, IEEE - 35th ECC, May 1985.
- [10] K. E. Felske and T. Moss, IEEE - 36th ECC, pp.641-648 (1986).
- [11] P. M. Hall, IEEE - 37th ECC, pp.579-588 (1987).
- [12] V. Brzozowski, et.al., FEA Analysis of Solder Joints, ManTech for ADSP, Monthly Report, March 20, 1987, Martin Marrietta Orlando Aerospace, Orlando, Florida.
- [13] H. D. Solomon, "Low-Cycle Fatigue of Surface Mounted Chip Carrier/Printed Wiring Board Joints," GE Report No. 87CRD185, Sept. 1987.
- [14] Hermetic Chip Carrier Compatible Printed Wiring Board, AFWAL-TR-85-4082, Westinghouse Defense Electronics Center, Baltimore, MD, July 1985.
- [15] WECAN - Westinghouse Electric Computer Analysis, USERS Manual, Westinghouse R&D Center, 1310 Beulah Road, Pittsburgh, PA 15235.

- [16] L. T. Greenfield and P. G. Forrester, "The Properties of Tin Alloys," Tin Research Institute, Greenford, England, 1961. As quoted in Solders and Soldering, H. H. Manko, McGraw-Hill, p.81 (1979).
- [17] M. B. Shamash, "Development of Highly Reliable Soldered Joints for Printed Circuit Boards," NTIS N69-25697, Westinghouse Defense and Space Center, Baltimore, 1968.